Applied Catalysis B: Environmental 201 (2017) 518–526

Contents lists available at ScienceDirect

Applied Catalysis B: Environmental

journal homepage: www.elsevier.com/locate/apcatb

A bio-inspired strategy to enhance the photocatalytic performance of g-C_3N_4 under solar irradiation by axial coordination with hemin

Xia Chen, Wangyang Lu*, Tiefeng Xu, Nan Li, Dandan Qin, Zhexin Zhu, Gangqiang Wang, Wenxing Chen*

National Engineering Lab for Textile Fiber Materials & Processing Technology (Zhejiang), Zhejiang Sci-Tech University, Hangzhou 310018, China, China

ARTICLE INFO

Article history:
Received 14 June 2016
Received in revised form 4 August 2016
Accepted 7 August 2016
Available online 24 August 2016

Keywords:
g-C_3N_4
Photocatalytic
Hemin
Biomimetic
Mechanism

ABSTRACT

In nature, metalloporphyrins, such as chlorophyll, cytochrome P450 and so forth, are key materials in maintaining the ecological cycles, especially the carbon cycle, and play an important role in both photosynthesis and the catalytic oxidation of organisms. Inspired by these factors, we skillfully combined photocatalysis and biomimetic catalysis using imidazole (IMD)-functionalized modification of g-C_3N_4 and axial coordination with hemin. Compared with pure hemin, g-C_3N_4 and a mixture of the two, our novel catalytic system (g-C_3N_4-IMD-hemin/H_2O_2) showed high photocatalytic oxidation activity for the degradation of 4-chlorophenol (4-CP), and the stability of hemin was enhanced under solar irradiation. Furthermore, the effect of pH and the sustained photocatalytic oxidation stability of g-C_3N_4-IMD-hemin for degrading 4-CP were investigated. The results indicated that g-C_3N_4-IMD-hemin presents a high photocatalytic oxidation activity over a wide pH range and exhibits good recyclability. A series of designed experiments showed that superoxide radicals ($^{\bullet}O_2^-$), high-valent iron (Fe(IV) = O) species, peroxy radicals ($^{\bullet}$OOH) and few hydroxyl radicals ($^{\bullet}$OH) were generated in the g-C_3N_4-IMD-hemin/H_2O_2 system. This synergistic photocatalytic and biomimetic process offers new insight for the utilization of solar energy and offers a new perspective for the exploration of catalysts for environmental remediation.

1. Introduction

Organic pollutants are widely dispersed in industrial wastewater and have caused widespread environmental concerns. Changing waste materials into energy has been a hot topic in science currently. Among the different recalcitrant organic pollutants, phenols are of particular concern because of their considerable toxicity and frequent industrial utilization [1,2]. Various technologies have been used for the treatment of phenols, including adsorption [3–8], biodegradation [9,10] and photocatalysis [11–14]. Graphitic carbon nitride (g-C_3N_4), as a metal-free polymeric photocatalyst with the advantages of being non-toxic, low in cost and thermally stable, has gained increasing attention in photocatalysis for the effective removal of phenols [15]. g-C_3N_4 can be easily prepared by the pyrolysis of urea and the different pyrolysis conditions influence its properties [16]. However, the fast charge recombination, poor absorption and low surface area of pure g-C_3N_4 have limited its application. So far, several diverse strategies have been explored to improve the photocatalytic activity of g-C_3N_4, including heteroatom doping [17,18], the construction of heterojunctions [19–21], copolymerization with other polymers [22] and dye sensitizing [23].

Unfortunately, the above approaches are confined to the modification of g-C_3N_4 in the field of photocatalysis. Conversely, there are few reports regarding the combination of photocatalysis and biomimetic catalysis, which is similar to the processes in ecological cycles. Hemin, an iron-porphyrin that has analogous π-conjugated structures to metallophthalocyanine, exhibits high biomimetic catalytic activity [24]. In particular, hemin has attracted attention for the purification of water [25]. However, the pure hemin in aqueous solution easily aggregates together to form catalytically inactive dimers, which has restricted its direct application [26–28]. Furthermore, in spite of its good performance in alkene epoxidation reactions [29,30], its application for the degradation of phenols has not been adequately explored because of its poor stability in reaction systems. To overcome these problems, two alternative approaches have been proposed. One approach is to modify the porphyrin rings with bulky functional groups for the protection of the iron porphyrin centers [31]. Another approach is to immobilize hemin on supports, such as graphene [32], titanium dioxide [33],

* Corresponding authors.
E-mail addresses: luwy@zstu.edu.cn (W. Lu), wxchen@zstu.edu.cn (W. Chen).

http://dx.doi.org/10.1016/j.apcatb.2016.08.020
0926-3373/

hydrogels [34], montmorillonite [35] or β-cyclodextrin [36]. It is noteworthy that the behavior of electron acceptance and donation between reactants and the central iron plays a crucial role for the catalytic activity of hemin. Therefore, choosing a suitable method that can change the electron transfer rate during the oxidation process might influence the catalytic activity of hemin.

On the basis of the above problems, we investigate a novel catalyst, g-C_3N_4-IMD-hemin, which is based on g-C_3N_4 functionalized with imidazole and then coupled with hemin through an axial ligand. In this catalyst, imidazole ligands are electron-donating groups that can change the electron transfer rate of the central iron and benefit the formation of high-valent iron species. This system cannot only be used to remove phenols and antibiotics, but also as a potential method for hydrogen generation. Moreover, the results show that the final degradation products are small biodegradable molecules. This synthetic technique is useful for the exploration of versatile catalysts for environmental remediation and energy conversion.

In order to investigate the photocatalytic properties of g-C_3N_4-IMD-hemin under solar irradiation, 4-chlorphenol (4-CP) was selected as the substrate and the degradation of antibiotics was also carried out. The results show that g-C_3N_4-IMD-hemin has good photocatalytic properties that can be maintained for a long time in a wide pH range. Additionally, to probe the active species during the catalytic oxidation process, an EPR spin trapping technique, high-definition electrospray mass spectra (ESI–MS) analyses, gas chromatography/mass spectrometry (GC–MS), isopropyl alcohol (IPA) and *p*-benzoquinone (PBQ) were utilized and the possible photocatalytic oxidation mechanism was proposed accordingly.

2. Experimental

2.1. Materials and reagents

Hemin, imidazole, dimethyl sulfone ($DMSO_2$) and PBQ were obtained from the Aladdin Chemistry Co. Ltd. 5-Bromovaleryl Chloride, 4-CP, 5,5-dimethyipyrroline-oxide (DMPO) and tetrahydrofuran anhydrous (dry THF) were purchased from the Tokyo Chemical Industry Co. Ltd. IPA and dimethyl sulfoxide (DMSO) were purchased from the Tianjin Wing Tai Chemical Co. Ltd. N,N-diethyl-1,4-phenylenediammonium sulfate (DPD) (AR, 98%) and peroxidase (POD) (specific activity ≥ 100 units mg^{-1}) were obtained from the Macklin Biochemical Technology Co. Ltd. Hydrogen peroxide (H_2O_2) was obtained from the Sinopharm Chemical Reagent Co. Ltd. Ultrapure water from a Milli-Q-Advantage A10 (Millipore) system was used in the experiments. All other solvents and chemicals used in the syntheses were of analytical grade and were used without further treatment.

2.2. Preparation of g-C_3N_4-IMD-hemin

Pristine g-C_3N_4 was obtained using a typical synthesis [37]. Urea (50 g) was placed in a crucible sealed with silver paper, and was heated to 550 °C for 3 h at a heating rate of 2.5 °C/min. Then the yellow powder was obtained after cooling. The g-C_3N_4-IMD-hemin photocatalyst was prepared by four steps and the synthetic process was described in Scheme 1. First, an environmental liquid exfoliation route was carried out by exfoliating g-C_3N_4 into ultrathin nanosheets in ultrapure water for 2 weeks, before being freeze-dried them for further use [38]. Then, the ultrasonic g-C_3N_4 power was dispersed in 100 ml of dry THF. 5-Bromovaleroyl chloride was dissolved in 50 ml of dry THF and added dropwise to the ultrasonic g-C_3N_4 dispersion over a period of 30 min under 0 °C. Aqueous ammonia (10 ml) was then added and reacted for 20 min. The solution was filtered, washed with ultrapure water and freeze-dried to obtain g-C_3N_4-Br. Furthermore, imidazole was dissolved in 100 ml of DMF and added to the g-C_3N_4-Br dispersion in 100 ml of DMF in the presence of K_2CO_3 for 8 h. The reaction was completed under a N_2 atmosphere in the dark. The solution was then centrifuged and washed with diethyl ether, ultrapure water respectively. The g-C_3N_4-IMD powder was collected after freeze-drying. Finally, g-C_3N_4-IMD and hemin were added to 200 ml of dry THF in the dark for 6 h. After the reaction, the solution was centrifuged, washed with ultrapure water and freeze-dried in order to collect the g-C_3N_4-IMD-hemin catalyst. The inductively-coupled plasma (ICP) technique was used to determine the mass fraction of hemin in g-C_3N_4-IMD-hemin (Fig. S1) with a value of 0.78% was obtained.

2.3. Characterization

X-ray diffraction (XRD) of the samples was performed using a DX-2700 X-ray diffractometer (Dandong Fangyuan, China) with Cu-Kα radiation. A UV–vis spectrometer (1J1-0015, HITACHI) was used to record UV–vis diffuse reflection spectra. UV–vis spectra were recorded using a UV–vis spectrometer. Fourier transform infrared spectroscopy (FT-IR) spectra were obtained using a Thermo Nicolet 5700 FTIR spectrometer with a wavenumber range of 4000–400 cm^{-1}. The thermogravimetric analysis (TGA) was completed using a TGA 1 (Mettler Toledo, Switzerland) with a heating rate of 10 °C/min. X-ray photoelectron spectroscopy (XPS) was conducted with a Thermo Scientific K-Alpha spectrometer (monochromatic Al Kα, 1486.6 eV). High-definition ESI–MS were collected using an ultra-performance liquid chromatography (UPLC)/Synapt G2-S HDMS system (Waters Q-TOF, USA).

2.4. Photocatalytic experiments

To investigate the photocatalytic performance of g-C_3N_4-IMD-hemin, 4-CP was selected as the substrate. The experiment was carried out in a 40 ml glass sample beaker with solar irradiation provided by a Q-Sun Xe-1 test chamber (USA) (Fig. S2). Before irradiation, g-C_3N_4-IMD-hemin (0.1 g/L) was dispersed in a 4-CP aqueous solution (5×10^{-5} mol/L) and treated by sonication. Furthermore, H_2O_2 was used as the oxidant. At given time intervals, the concentration of 4-CP was detected by UPLC equipped with the Acquity BEH C18 column (1.7 μm, 2.1 × 50 mm, Waters). NaOH or H_2SO_4 were used to adjust the pH of the reaction system and the experiment was carried out at ambient temperature and atmospheric pressure.

The transient photocurrent responses of the samples were studied with an electrochemical analyzer (CHI660E, China) with a 100 W lamp (LOT-oriel GmbH & Co. KG) as the light source. The carbon papers dip-coated with the samples were served as the working electrodes that were prepared as follows: 2 mg of catalyst was added into the solution with isopropanol, ultrapure water and perfluorosulfonic acid polymer (Nafion), mixed at a certain proportion, then, the prepared slurry was dip-coated onto the carbon paper with a range of 1 × 5 cm and dried for further use. The counter electrode was employed using a Pt wire and the reference electrode was prepared with Ag/AgCl (saturated KCl).

2.5. Analytical methods

The photocatalytic degradation products of 4-CP were detected by UPLC/Synapt G2-S HDMS (Waters Q-TOF, USA) analyses which was equipped Metabolynx xs system. Data acquisition and instrument control were performed by Micromass MassLynx software and the corresponding parameters for the UPLC/Synapt G2-S HDMS analyses were with ESI negative ion mode, lock mass correction of leucine enkephalin (LE, Tyr-Gly-Gly-Phe-Leu, negative *m/z* 554.2615) and the scan range was set to 40–800 *m/z*. In negative

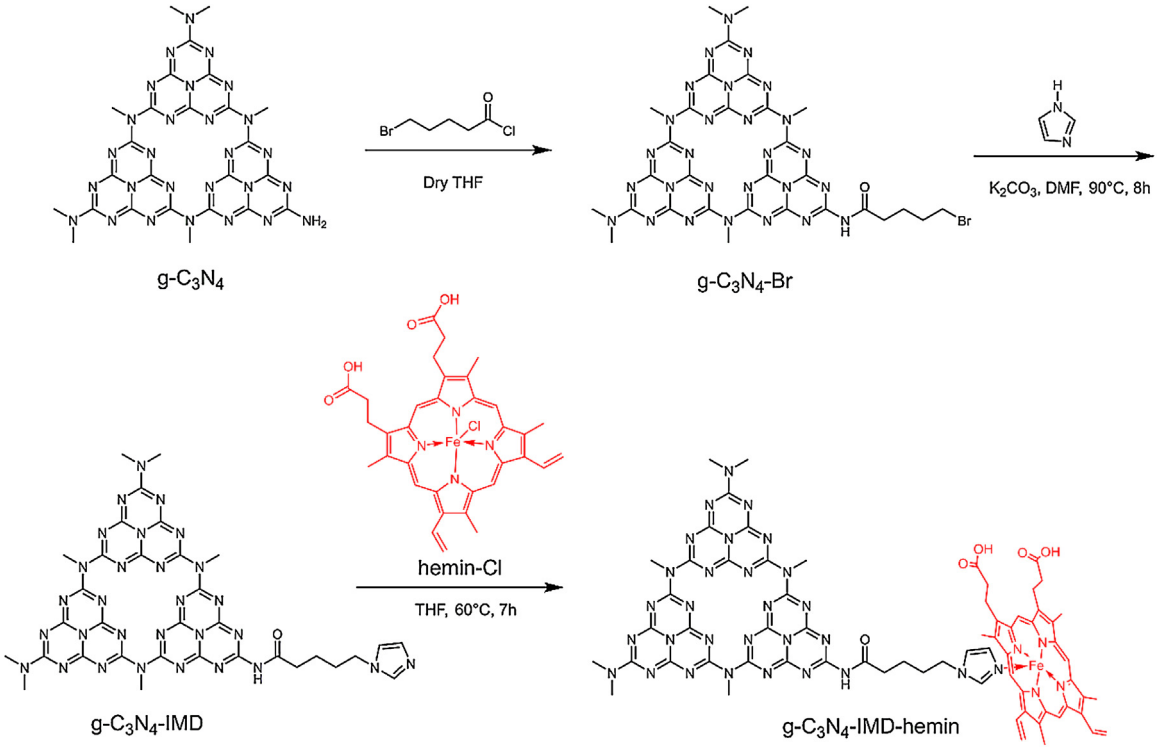

Scheme 1. Synthesis of g-C_3N_4-IMD-hemin.

mode, the final degradation solution of 4-CP was freeze-dried and the conditions of 4-CP were a capillary voltage of 3 kV, a sample cone voltage of 40 V, a source temperature of 150 °C and a desolvation temperature of 500 °C. High purity nitrogen gas was used as the cone and desolvation gas at rates of 50 and 500 l/h, respectively. A 2 μl solution was injected into a HSS T3 column (1.8 μm × 100 mm) using the auto sampler. The flow rate was 0.3 ml/min and the column oven temperature was set to 35 °C. The mobile phases of the final degradation products were as follows: A: 0.1% formic acid + 99.9% H_2O, B: 100% methanol. The gradient elution began with 99% A for 0.2 min, followed by a decrease to 80% A at 6 min, and in the next 2.5 min it remained at 40% A.

The designed experiments for detecting high-valent iron (Fe(IV) = O) species were carried out by gas chromatography/mass spectrometry (GC–MS, GC: Agilent 6890 N equipped with a OV1701 capillary column 30 m × 0.25 mm × 0.25 μm, MS: Agilent 5973i) and UPLC/Synapt G2-S HDMS (Waters Q-TOF, USA) in positive mode.

3. Results and discussion

3.1. Characterization

As shown in Fig. S3, the UV–vis spectrum of the hemin solution contains an absorption peak at about 398 nm. In addition, compared with pure g-C_3N_4, g-C_3N_4-Br and g-C_3N_4-IMD, g-C_3N_4-IMD-hemin shows better absorption in the wavelength range of 450–550 nm (Fig. 1). This result is attributed to the absorption of trace amounts of hemin in g-C_3N_4-IMD-hemin. Based on the above analysis, the coordinated interaction between g-C_3N_4-IMD and hemin might enhance the photocatalytic properties of g-C_3N_4.

The chemical structures of the samples were further confirmed by FT-IR spectra (Fig. S4). The broad absorption bands between 3300 and 3100 cm^{-1} are assignable to the uncondensed amine groups and intermolecular hydrogen-bonding interactions [37,39,40]. The bands in the range of 1600–1200 cm^{-1} are mainly

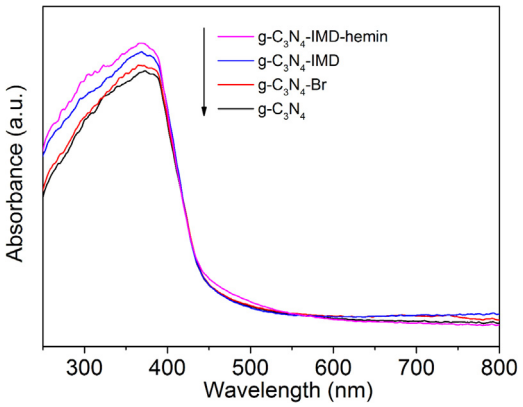

Fig. 1. UV–vis diffuse reflectance absorption spectra of g-C_3N_4, g-C_3N_4-Br, g-C_3N_4-IMD and g-C_3N_4-IMD-hemin.

due to the typical vibrations of aromatic carbon nitride heterocycles and the bands at 880–800 cm^{-1} are ascribed to the triazine units [16,41]. Furthermore, the multiple peaks of g-C_3N_4, g-C_3N_4-Br, g-C_3N_4-IMD and g-C_3N_4-IMD-hemin remain almost unchanged, which suggests that the bulk structure and chemical skeleton of g-C_3N_4 have not been severely altered. However, the intensity of g-C_3N_4-IMD and g-C_3N_4-IMD-hemin peaks are strengthened gradually in the region of 1600–1200 cm^{-1} which can be attributed to the imidazole and hemin content.

XPS was used to show the coordinated interaction between g-C_3N_4 and hemin. As demonstrated in Fig. 2, the C 1s peaks at 288.0–288.7 eV correspond to the C—N—C coordination and the sp^2 hybridized carbon in the N-containing aromatic ring (N—C=N), while the binding energies at 286.0–286.4 eV are ascribed to the C—NH_2 species and the peaks at 284.5–284.6 eV are attributed to the sp^2 C—C bonds [42–44]. For hemin, the C 1s peak at 287.1 eV is ascribed to the C=O species. As can be seen in Fig. 2, compared with the C—C peak, the N—C=N and C—NH_2 peaks of g-C_3N_4-IMD-hemin

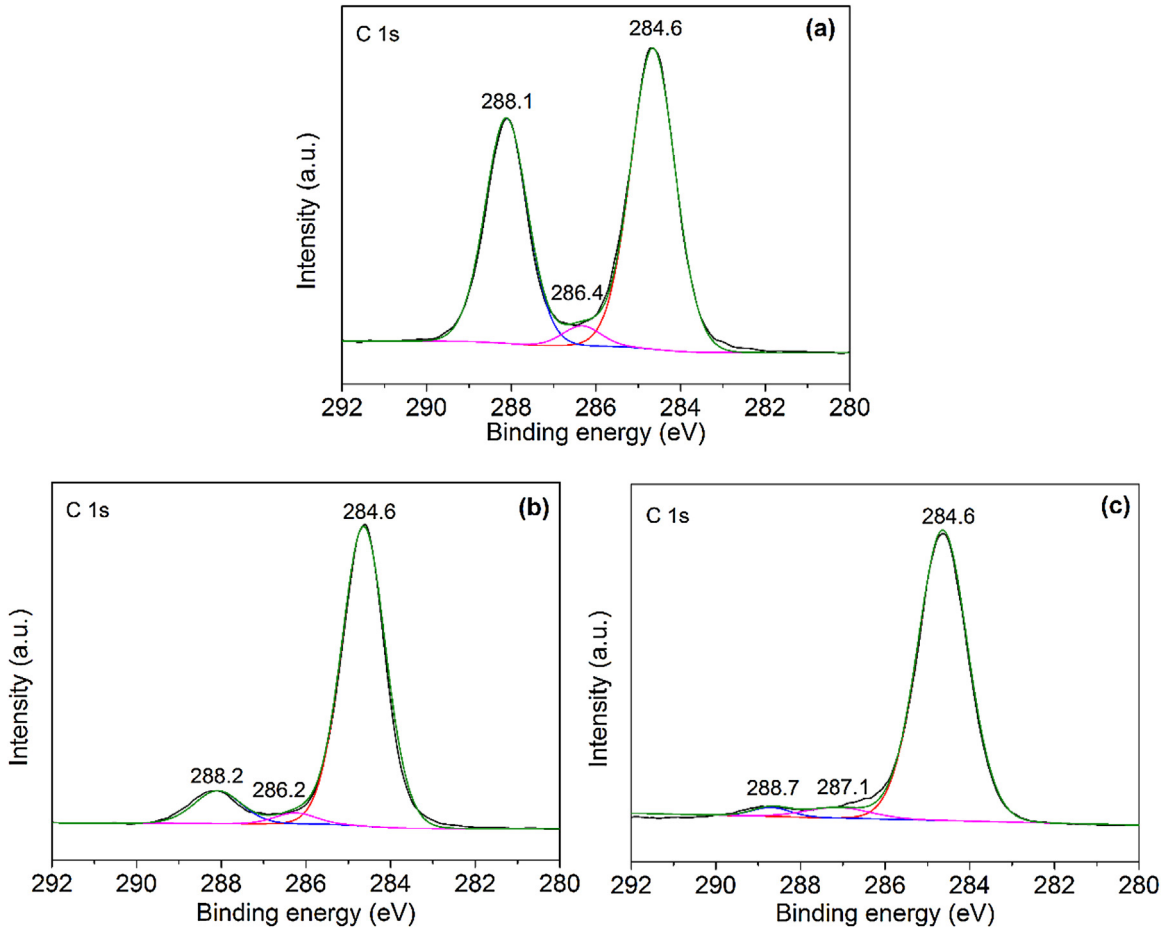

Fig. 2. Curve fit of the C 1s peak of (a) g-C_3N_4, (b) g-C_3N_4-IMD-hemin and (c) hemin.

are reduced. This might be attributed to the amidation reaction between g-C_3N_4 and 5-Bromovaleryl Chloride, and the coordinated interaction between g-C_3N_4 and hemin, which lead to the decrease in N—C═N bonds and the increase in C—C bonds. Fig. S5 shows the peaks detected in the N 1s spectra. The main N 1s XPS of g-C_3N_4 at 398.5 eV is ascribed to the sp^2-hybridized nitrogen (C═N—C) in the triazine rings, and the N 1s XPS of hemin at 398.5 eV can be attributed to the four chemically equivalent N atoms which bind to the central iron atom of the porphyrin ring [45–47]. Meanwhile, for g-C_3N_4-IMD-hemin, the peak of N 1s at 400.0–400.1 eV, originating from N-$(C)_3$ groups, is reduced and the peak at 401.1 eV, assigned to the nitrogen of the amide group (—NH—CO—), is increased compared with the peak at 398.5 eV. The above results indicate that hemin has been successfully immobilized on g-C_3N_4.

We employed ESI-MS to further show that the imidazole ligands were successfully coordinated onto hemin. As shown in Fig. 3, 1-butylimidazole, which has a similar structure to the complex of imidazole and 5-Bromovaleryl Chloride, was employed in this study. The ESI-MS results reveal three prominent ions at mass/charge (m/z) ratios of 125.1075, 616.1766 and 740.2737, which correspond to the ions formed by 1-Butylimidazole, hemin and the complex of hemin and 1-butylimidazole. From this analysis, we can assume that the imidazole ligands have been coordinated onto hemin successfully.

The XRD patterns of the samples are shown in Fig. S6. For the pure g-C_3N_4, two distinct peaks at 27.5° and 13.1° are found, which corresponds to the (002) and (100) planes, respectively (JCPDS No. 87-1526). The diffraction peaks at 27.5° and 13.1° correspond to interplanar separations of 0.324 and 0.682 nm, respectively. It can be seen that the diffraction peaks of g-C_3N_4-IMD-hemin are very similar to pure g-C_3N_4, which may be ascribed to the fact that there is a small quantity of hemin content in g-C_3N_4-IMD-hemin.

Moreover, to investigate the thermal stability of g-C_3N_4-IMD-hemin, TGA was employed. As shown in Fig. 4, the curves of g-C_3N_4 and g-C_3N_4-Br display a low weight loss from 300 to 450 °C, which is attributed to the loss of surface water. However, when the temperature is above 450 °C, the pure g-C_3N_4 and g-C_3N_4-Br show weight loss at different temperatures and the final degradation processes are accomplished at about 720 and 670 °C, respectively. As for g-C_3N_4-IMD, the weight loss at 150 °C is due to the decomposition of imidazole substituents. This result can be used to prove that the imidazole is successfully grafted to the g-C_3N_4-Br. However, the amount of hemin in the photocatalyst is very low, so hemin (4.8 mg) is used for the test. Furthermore, the pure hemin exhibits two weight-loss steps on the TG curves. For g-C_3N_4-IMD-hemin, a good thermal stability until 500 °C is observed, resulting from the successful coordination interaction between g-C_3N_4-IMD and hemin.

3.2. Photocatalytic activity

In this study, we chose 4-CP as the substrate to evaluate the photocatalytic activities of different samples. First, the influence of the amount of hemin on the photocatalytic activity under the same conditions was investigated. As shown in Fig. S7, the removal rate of 4-CP using g-C_3N_4-IMD-hemin was higher than that of pure hemin or g-C_3N_4, and it improved with the increase of the hemin amount. When the feed ratio of hemin and g-C_3N_4 reached 2.00% or 5.00%,

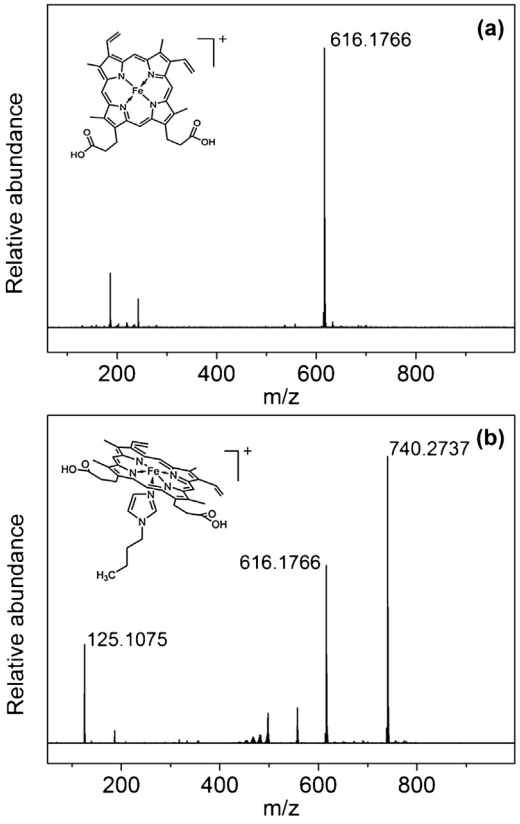

Fig. 3. High-definition electrospray mass spectra of (a) hemin and in the presence of (b) 1-Butylimidazole.

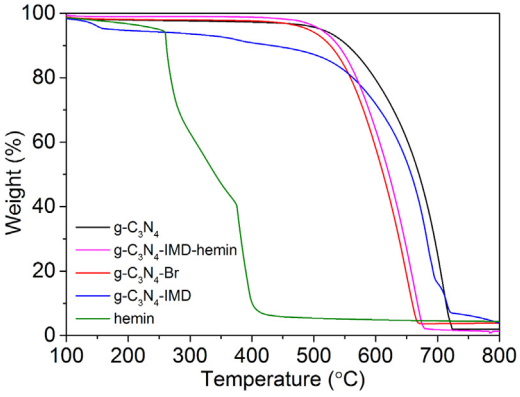

Fig. 4. Thermogravimetric analysis of g-C_3N_4, g-C_3N_4-Br, g-C_3N_4-IMD, g-C_3N_4-IMD-hemin and hemin.

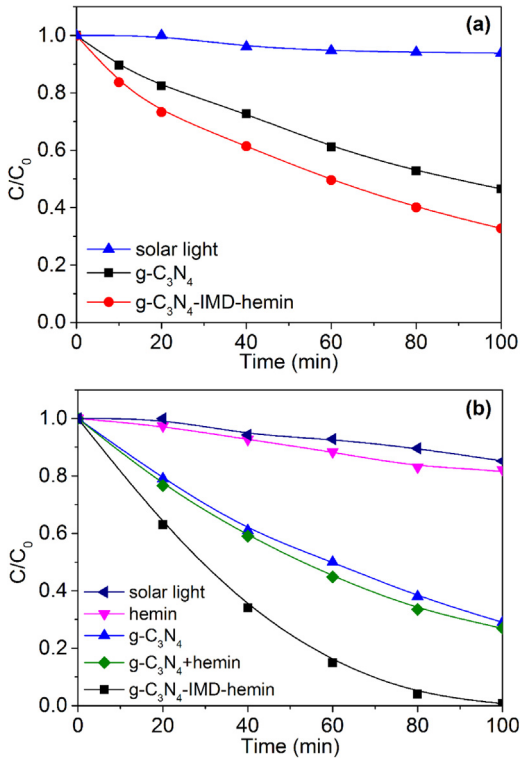

Fig. 5. (a) Photocatalytic degradation of 4-CP (5×10^{-5} mol/L) in the presence of g-C_3N_4 and g-C_3N_4-IMD-hemin under solar irradiation. [g-C_3N_4] = 0.1 g/L, [g-C_3N_4-IMD-hemin] = 0.1 g/L, pH 9. (b) Photocatalytic degradation of 4-CP (5×10^{-5} mol/L) in the presence of g-C_3N_4, g-C_3N_4-IMD-hemin, hemin and g-C_3N_4 + hemin under solar irradiation. [g-C_3N_4] = 0.1 g/L, [g-C_3N_4-IMD-hemin] = 0.1 g/L, [hemin] = 0.1 g/L, [g-C_3N_4 + hemin] = 0.1 g/L, [H_2O_2] = 10 mM, pH 9.

it exhibited the highest photocatalytic performance. The results indicated that too much hemin was useless in the system so that g-C_3N_4-IMD-hemin (2.00%) was chosen to study the performance of g-C_3N_4-IMD-hemin. As shown in Fig. 5a the concentration of 4-CP showed no obvious change in the presence of solar irradiation without H_2O_2 and the catalyst. When H_2O_2 was used (Fig. 5b), there was no obvious change too. This indicated that solar irradiation was not sufficiently powerful to degrade 4-CP. In addition, hemin/H_2O_2 also showed a low photocatalytic activity with a removal percentage of 18% that was due to molecular aggregation of hemin, resulting in catalytically inactive dimers and oxidative self-destruction in the reaction system (Fig. 6a). Furthermore, as demonstrated in Fig. 6b, hemin functionalized with imidazole ligands also exhibited a low stability in the process of solar irradiation, suggesting that small molecular porphyrin easily to oxidative self-destruction without support. For g-C_3N_4 and g-C_3N_4-IMD-hemin without H_2O_2, the removal percentages of 4-CP were about 53% and 68%, respectively. However, in the presence of g-C_3N_4-IMD-hemin/H_2O_2, the degradation of 4-CP was complete. For g-C_3N_4/H_2O_2, the removal rate of 4-CP was 70%, which was similar to the mixture of g-C_3N_4 and hemin (g-C_3N_4 + hemin) with H_2O_2 and g-C_3N_4-IMD-hemin without H_2O_2. Based on these results, the synergistic biomimetic photocatalytic effect between g-C_3N_4 and hemin enhanced the performance of the system. Furthermore, to investigate the effect of imidazole ligands, a control test of g-C_3N_4 + hemin with and without imidazole ligands was carried out. As shown in Fig. S8, the photocatalytic activity was enhanced in the presence of imidazole, which indicated that imidazole played an important role in the catalyst. However, the mixture of g-C_3N_4 and hemin showed a poor recyclability (Fig. S12). Therefore, it is necessary to combine hemin with g-C_3N_4 by axial imidazole ligands. In addition, compared with the photocatalytic performance showed in Fig. 5 and Fig. S12, the enhanced activity presented in Fig. S8 can be related to the amount of hemin in this part is four times than the amount in Fig. 5 and Fig. S12 and the effect of homogeneous phase of hemin.

The effects of pH value and H_2O_2 concentration were also investigated. The results for the photocatalytic degradation of 4-CP in the presence of g-C_3N_4 and g-C_3N_4-IMD-hemin at different pH values are presented in Fig. 7. For g-C_3N_4-IMD-hemin, complete degradation of 4-CP was displayed, regardless of whether it was in acidic, neutral and alkaline conditions. However, g-C_3N_4 only presented high photocatalytic performance in acidic conditions (pH 5), with poor photocatalytic performance being exhibited at pH 7 and 9. Therefore, g-C_3N_4-IMD-hemin exhibited a higher photocatalytic activity than g-C_3N_4 over a wider pH range. In addition, to explore the influence of H_2O_2, the photogenerated H_2O_2 content during the

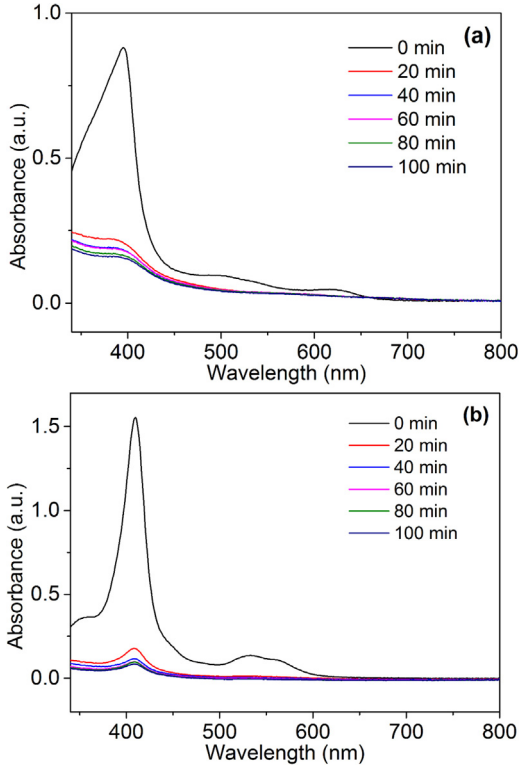

Fig. 6. UV–vis spectra of solutions of (a) hemin and (b) hemin functionalized with imidazole ligands in the process of solar irradiation. [H_2O_2] = 10 mM, pH 9.

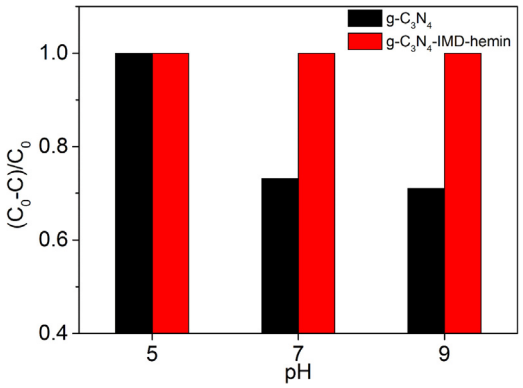

Fig. 7. Removal rate for the photocatalytic degradation of 4-CP (5×10^{-5} mol/L) at different pH values in the presence of g-C_3N_4 and g-C_3N_4-IMD-hemin under solar irradiation. [g-C_3N_4] = 0.1 g/L, [g-C_3N_4-IMD-hemin] = 0.1 g/L, [H_2O_2] = 10 mM.

reaction without an excess addition of H_2O_2 was detected by a photometric method based on the POD-catalyzed oxidation by H_2O_2 of DPD [48]. The absorption spectra of the DPD/POD reagent after reaction with H_2O_2 produced from the reaction system is shown in Fig. S9. The H_2O_2 concentrations at given time intervals were calculated by combining the standard curve of the DPD/POD method (Fig. S10) with the absorbance of the DPD/POD reagent at 551 nm. As can be seen, the content of H_2O_2 was enhanced gradually during the reaction, but the dosage produced from the reaction system was not enough for the degradation of 4-CP. For this case, it was necessary to add extra H_2O_2 and the decomposition amount of 4-CP increased with an increase in the H_2O_2 dosage, as demonstrated in Fig. S11. Additionally, the final biomimetic photocatalytic oxidation products are presented in Table S1. Good recyclability for g-C_3N_4-IMD-hemin was observed and the results are presented in Fig. S12. However, g-C_3N_4 + hemin showed a poor recyclability

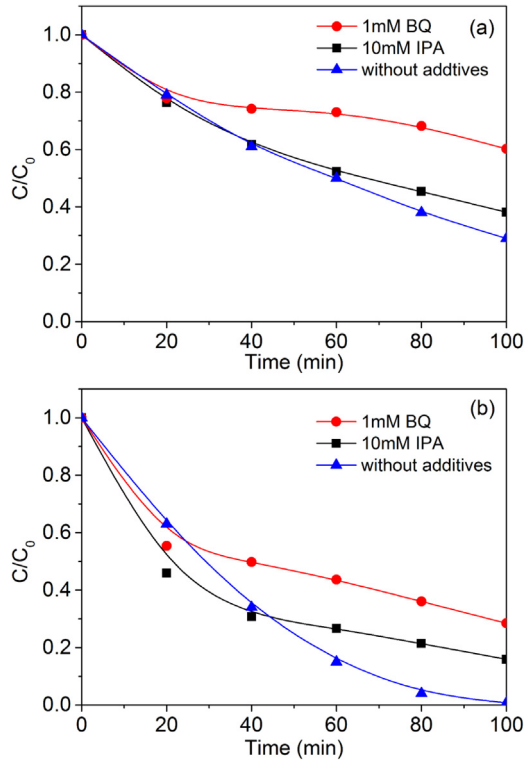

Fig. 8. Effect of trapping agents on photocatalytic degradation of 4-CP (5×10^{-5} mol/L) under solar irradiation with (a) g-C_3N_4 and (b) g-C_3N_4-IMD-hemin. [g-C_3N_4-IMD-hemin] = 0.1 g/L, [g-C_3N_4] = 0.1 g/L, [H_2O_2] = 10 mM, pH 9.

which could be assigned to that hemin in aqueous solution easily aggregates together to form catalytically inactive dimers. Several other pollutants are listed in Table S2. According to the above results, the stability of hemin was enhanced in the g-C_3N_4-IMD-hemin/H_2O_2 system and the introduction of hemin might result in the formation of various active species, different to pure g-C_3N_4 and bulk hemin. This result is significant for wastewater treatment and energy conversion.

3.3. Mechanism analysis

To investigate the active species during the reaction process, PBQ and IPA were added to determine whether superoxide ($^{\bullet}O_2^-$) and hydroxyl radicals ($^{\bullet}OH$) were the active species in the photocatalytic degradation of 4-CP. As shown in Fig. 8a, the removal rate of 4-CP had no obvious decrease in the existence of IPA, which indicated that $^{\bullet}OH$ was not the dominating active species in the photocatalytic reaction with g-C_3N_4. However, the decomposition of 4-CP was inhibited significantly in the presence of BQ, suggesting that $^{\bullet}O_2^-$ was the main active species in the system of g-C_3N_4/H_2O_2. For the system of g-C_3N_4-IMD-hemin/H_2O_2, $^{\bullet}O_2^-$ is the main effective active species in the degradation process of 4-CP (Fig. 8b), simultaneously with $^{\bullet}OH$.

An EPR spin trapping technique (with DMPO) was adopted to further study the current reaction mechanism. As demonstrated in Fig. S13a, no obvious DMPO-$^{\bullet}OH$ signal was detected in the g-C_3N_4-IMD-hemin without H_2O_2 system, which indicated that the hydroxyl radical was not the main active species in the system. In methanol solution, the DMPO-$^{\bullet}OOH$ signal was detected in the g-C_3N_4-IMD-hemin without H_2O_2 system (Fig. S13b), implying that $^{\bullet}OOH$ played a main role in this photocatalytic system. At the same time, Fig. 9a showed weak EPR signals of DMPO-$^{\bullet}OH$ in the g-C_3N_4-IMD-hemin/H_2O_2 system. With regard to the g-C_3N_4-IMD-hemin/H_2O_2 system, the formation of DMPO-$^{\bullet}OOH$ species was also

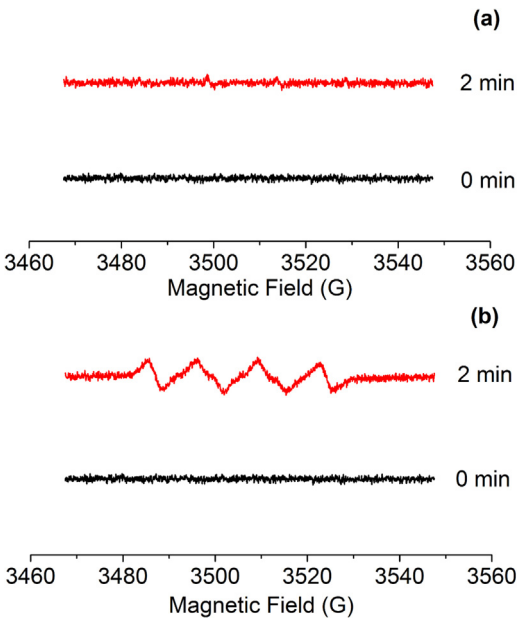

Fig. 9. DMPO spin-trapping EPR spectra in aqueous or methanol solutions in the presence of g-C_3N_4-IMD-hemin under solar irradiation, (a) aqueous solution and (b) methanol solution. [DMPO] = 10 mM, [H_2O_2] = 10 mM, pH 9.

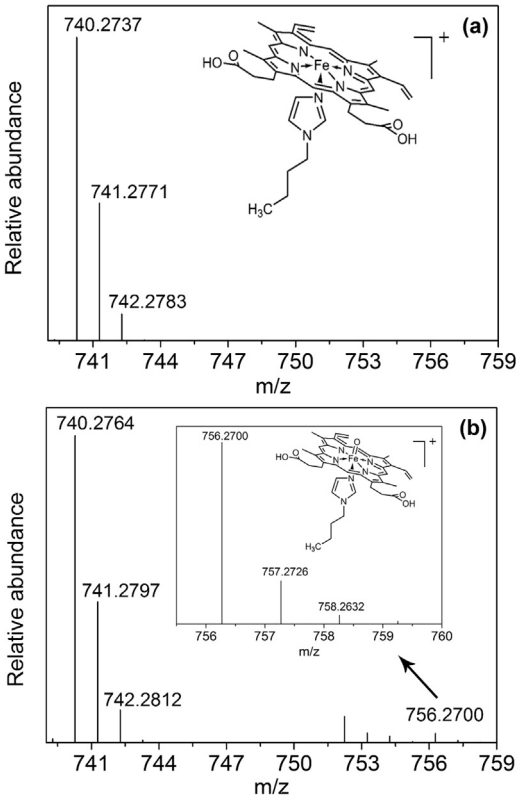

Fig. 10. High-definition electrospray mass spectra of hemin functionalized with (a) 1-Butylimidazole and in the presence of (b) H_2O_2.

detected in methanol solution (Fig. 9b). From these results, it can be concluded that •OH, •OOH and $•O_2^-$ were all involved in the photocatalytic degradation reaction of the g-C_3N_4-IMD-hemin/H_2O_2 system.

Experiments were carried out to detect other possible active species in the photocatalytic oxidization of 4-CP. Sulfoxides (e.g., DMSO, methyl phenyl sulfoxide and methyl *p*-tolyl sulfoxide) can react with Fe(IV) = O species through a two-electron transfer process to produce the corresponding sulfones (reaction 1), which differed observably from the •OH-involved products (reaction (2)) [49,50].

$$Fe(IV) = O + (CH_3)_2SO \rightarrow (CH_3)_2SO_2 \quad (1)$$

$$2•OH + 2(CH_3)_2SO + O_2 \rightarrow 2CH_3SO_2H + HCHO + CH_3OH \quad (2)$$

As shown in Fig. S14, a signal peak of a standard sample emerged at 5.14 min and a similar peak of g-C_3N_4-IMD-hemin in methanol solution with the same retention time was detected.

As further evidence, an ESI–MS analysis of the complexes was carried out [51,52]. As shown in Fig. 10b, ESI–MS studies of hemin functionalized with 1-butylimidazole in the presence of H_2O_2 revealed one ion signal at a *m*/*z* ratio of 756.2700 with an admissible error value of 2.3 mDa, which corresponded to a complex with 1-butylimidazole coordinated to the hemin and the central iron oxidized by H_2O_2. This signal was not detected in the system of Fig. 10a without H_2O_2. From these results, we can infer that the system of g-C_3N_4-IMD-hemin/H_2O_2 had Fe(IV) = O species.

Based on all the experimental results, a speculative photocatalytic mechanism for the degradation of phenols and antibiotics using g-C_3N_4-IMD-hemin/H_2O_2 is proposed in Fig. 11. According to the literature [53,54], in the presence of H_2O_2, the original formation of Fe(III) in hemin is transformed into an end-on Fe^{III}-OOH species. However, the hydrogen peroxide O—O bond can be cleaved both homolytically and heterolytically, depended on the conditions, such as the electronic properties of the axial ligands, iron porphyrin complexes, solvents and the surrounding conditions of the O—O bond [55]. When the substituent groups or axial ligands of the porphyrin ring are electron donating groups or there are electron withdrawing groups around the O—O bond, it is beneficial for the O—O bond to be cleaved heterolytically, whereas it is conducive to the homolysis of H_2O_2 when the substituent groups or axial ligands of the porphyrin ring are electron withdrawing groups or there are electron donating groups around the O—O bond. According to our analysis, in the g-C_3N_4-IMD-hemin/H_2O_2 system, heterolytic cleavage of the O—O bond plays a significant role in the decomposition of H_2O_2 with active species of Fe(IV) = O. This can be attributed to the fact that the imidazole ligands are electron donating groups which accelerate the heterolysis of H_2O_2 and promote the formation of Fe(IV) = O. Furthermore, the photogenerated electrons and hole pairs of g-C_3N_4 were excited synchronously under solar light irradiation. The photogenerated electrons from the conduction band of g-C_3N_4 could react with dissolved oxygen in the system to form $•O_2^-$, which could react with H^+ and be converted into •OOH reversibly. Meanwhile, when the disproportionation of $•O_2^-$ or the one electron reduction appeared on the formation of H_2O_2, it could react with the electron on the conduction band and produced •OH [56,57]. These findings demonstrate that Fe(IV) = O, $•O_2^-$, •OOH and small amounts of •OH all contribute to the photocatalytic degradation of phenols and antibiotics in the presence of g-C_3N_4-IMD-hemin and H_2O_2. The result is in good agreement with the experimental results.

Photocurrent technology was employed to demonstrate the charge separation efficiency in the photocatalysts and provide further evidence to support the viewpoints given previously [58,59]. As shown in Fig. 12, both g-C_3N_4 and g-C_3N_4-IMD-hemin showed a preferable response to UV–vis light provided by a 100 W lamp (LOT-oriel GmbH & Co. KG). Furthermore, the transient photocurrent density response under visible light ($\lambda > 400$ nm) was also measured for the samples (Fig. S15). Compared with pure g-C_3N_4, the photocurrent density response of g-C_3N_4-IMD-hemin had a slight weak value with 0.02 μA which could be attributed to the grafted groups on the surface of g-C_3N_4 might have some impact on the efficiency of charge separation. Meanwhile, the results also suggested

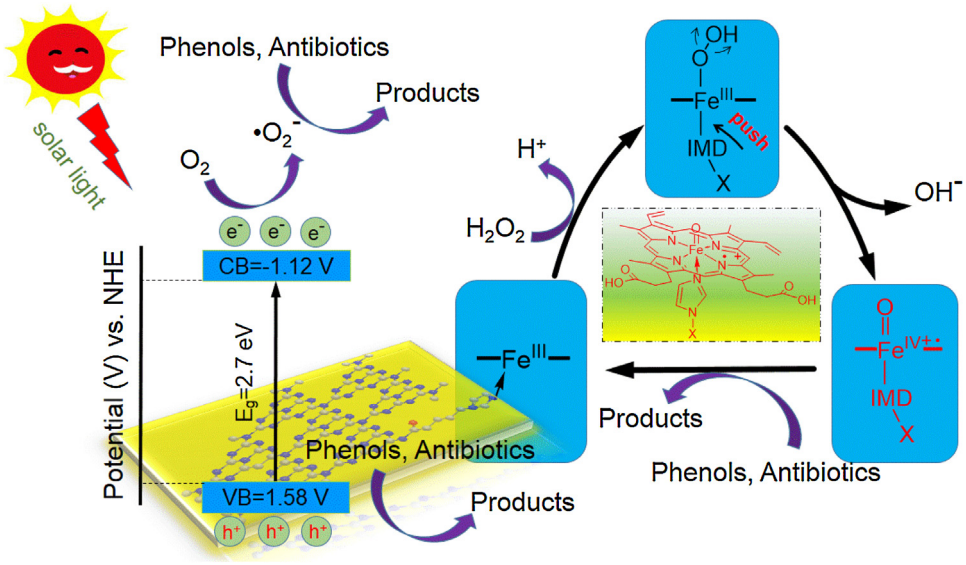

Fig. 11. Possible reaction mechanism over the g-C_3N_4-IMD-hemin photocatalyst under solar irradiation.

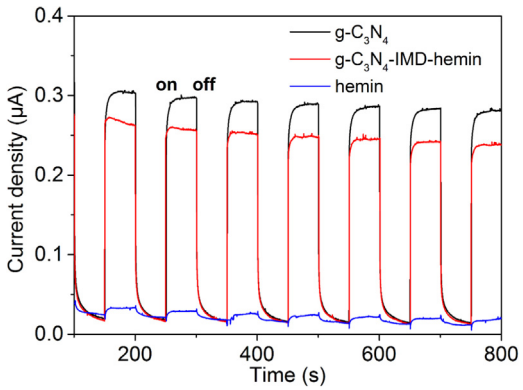

Fig. 12. Transient photocurrent density response of g-C_3N_4, g-C_3N_4-IMD-hemin and hemin photocatalyst electrodes with light on-off cycles under UV–vis light irradiation. [Na_2SO_4] = 0.1 M.

that the hemin had little influence on the photogenerated electron-hole pairs of g-C_3N_4 and the electron-hole recombination rate was lower in the g-C_3N_4-IMD-hemin/H_2O_2 system. These results were consistent with the information obtained from the sensitive EPR spectra (Fig. S16). The intensities of EPR were enhanced when g-C_3N_4 and g-C_3N_4-IMD-hemin samples were irradiated with UV–vis light or visible light compared with the samples in the dark. For the single-line EPR spectrum (g = 2.0031), it is attributed to the generated conduction electrons coming from the localized π states of g-C_3N_4 [60,61].

4. Conclusions

In summary, we reported a novel synergistic photocatalytic and biocatalytic system for removing 4-CP and antibiotics using a g-C_3N_4-IMD-hemin catalyst in the presence of H_2O_2 under solar irradiation. The imidazole acted as an axial ligand which connected hemin to g-C_3N_4, promoting the O—O bond to be cleaved heterolytically to generate active Fe(IV) = O species. The strong coordinate bond between g-C_3N_4 and hemin played an important way in enhancing the stability of hemin and the photocatalytic oxidation performance of g-C_3N_4, which were ascribed to a suitable microenvironment provided by g-C_3N_4 and the "push" effect of imidazole for hemin. Furthermore, the photocatalytic oxidation performance of g-C_3N_4-IMD-hemin was higher than the mixture sample of g-C_3N_4 and hemin. Meanwhile, a good recyclability and a wide pH tolerance were attributed to the formation of Fe(IV) = O, $^{\bullet}O_2^-$, $^{\bullet}$OOH and $^{\bullet}$OH. More importantly, the final degradation products of 4-CP were determined as biodegradable small molecules. Therefore, this work provides a new insight into the degradation of recalcitrant pollutants, which is beneficial to exploring new photocatalytic oxidation catalysts for environmental remediation and energy conversion.

Author contributions

The manuscript was written through contributions of all authors. All authors have given approval to the final version of the manuscript.

Notes

The authors declare no competing financial interest.

Acknowledgments

This work was supported by the National Natural Science Foundation of China (No. 51133006 and 51103133), Zhejiang Provincial Natural Science Foundation of China (No. LY14E030013), the Public Technology Application Research Project of Zhejiang Province (NOs. 2015C33018 and 2016C33019), Textile Vision Science & Education Fund, and 521 Talent Project of ZSTU.

Appendix A. Supplementary data

Supplementary data associated with this article can be found, in the online version, at http://dx.doi.org/10.1016/j.apcatb.2016.08.020.

References

[1] S. Lacorte, I. Guiffard, D. Fraisse, D. Barcelo, Anal. Chem. 72 (2000) 1430–1440.
[2] A. Zemann, D. Volgger, Anal. Chem. 69 (1997), 3243–1440.
[3] J.D. Snyder, J.G. Leesch, Ind. Eng. Chem. Res. 40 (2001) 2925–2933.
[4] H.L. Wang, W.F. Jiang, Ind. Eng. Chem. Res. 46 (2007) 5405–5411.
[5] A.A. El-Feky, M.N. Shalaby, Polym. Adv. Technol. 14 (2003) 12–18.
[6] M.K. Abu-Arabi, M.A. Allawzi, A.S. Al-Zoubi, Chem. Eng. Technol. 30 (2007) 493–500.

[7] M. Khalid, G. Joly, A. Renaud, P. Magnoux, Ind. Eng. Chem. Res. 43 (2004) 5275–5280.
[8] B. Pan, W. Du, W. Zhang, X. Zhang, Q. Zhang, B. Pan, L. Lv, Q. Zhang, J. Chen, Environ. Sci. Technol. 41 (2007) 5057–5062.
[9] T. Chung, P. Wu, R. Juang, Biotechnol. Bioeng. 87 (2004) 219–227.
[10] S.S. Adav, M. Chen, D. Lee, N. Ren, Biotechnol. Bioeng. 96 (2007) 844–852.
[11] I. Oller, W. Gernjak, M.I. Maldonado, L.A. Perez-Estrada, J.A. Sanchez-Perez, S. Malato, J. Hazard. Mater. 138 (2006) 507–517.
[12] A. Garcia-Ripoll, A.M. Amat, A. Arques, R. Vicente, M.F. Lopez, I. Oller, M.I. Maldonado, W. Gernjak, Chemosphere 68 (2007) 293–300.
[13] W. Lu, T. Xu, Y. Wang, H. Hu, N. Li, X. Jiang, W. Chen, Appl. Catal. B: Environ. 180 (2016) 20–28.
[14] M.A. Barakat, J.M. Tseng, C.P. Huang, Appl. Catal. B: Environ. 59 (2005) 99–104.
[15] X. Wang, S. Blechert, M. Antonietti, ACS Catal. 2 (2012) 1596–1606.
[16] F. Dong, Z. Zhao, T. Xiong, Z. Ni, W. Zhang, Y. Sun, W.K. Ho, ACS Appl. Mater. Interfaces 5 (2013) 11392–11401.
[17] X. Chen, J. Zhang, X. Fu, M. Antonietti, X. Wang, J. Am. Chem. Soc. 131 (2009) 11658–11659.
[18] G. Liu, P. Niu, C. Sun, S.C. Smith, Z. Chen, G.Q. Lu, H.M. Cheng, J. Am. Chem. Soc. 132 (2010) 11642–11648.
[19] C. Pan, J. Xu, Y. Wang, D. Li, Y. Zhu, Adv. Funct. Mater. 22 (2012) 1518–1524.
[20] H. Li, J. Liu, W. Hou, N. Du, R. Zhang, X. Tao, Appl. Catal. B: Environ. 160–161 (2014) 89–97.
[21] S. Wang, D. Li, C. Sun, S. Yang, Y. Guan, H. He, Appl. Catal. B: Environ. 144 (2014) 885–892.
[22] J. Zhang, X. Chen, K. Takanabe, K. Maeda, K. Domen, J.D. Epping, X. Fu, M. Antonietti, X. Wang, Angew. Chem. Int. Ed. 49 (2010) 441–444.
[23] S. Min, G. Lu, J. Phys. Chem. C 116 (2012) 19644–19652.
[24] Y. Yao, Y. Mao, Q. Huang, L. Wang, Z. Huang, W. Lu, W. Chen, J. Hazard. Mater. 264 (2014) 323–331.
[25] S. Pirillo, F.S.G. Einschlag, E.H. Rueda, M.L. Ferreira, Ind. Eng. Chem. Res. 49 (2010) 6745–6752.
[26] T.C. Bruice, Acc. Chem. Res. 24 (1991) 243–249.
[27] S. Deng, J. Lei, Y. Huang, Y. Cheng, H. Ju, Anal. Chem. 85 (2013) 5390–5396.
[28] Y. Zang, J. Lei, L. Zhang, H. Ju, Anal. Chem. 86 (2014) 12362–12368.
[29] P.S. Coelho, E.M. Brustad, A. Kannan, F.H. Arnold, Science 339 (2013) 307–310.
[30] A.C. Serra, C. Docal, A.M.d.A. Rocha Gonsalves, J. Mol. Catal. A: Chem. 238 (2005) 192–198.
[31] M. Shema-Mizrachi, G.M. Pavan, E. Levin, A. Danani, N.G. Lemcoff, J. Am. Chem. Soc. 133 (2011) 14359–14367.
[32] T. Xue, S. Jiang, Y. Qu, Q. Su, R. Cheng, S. Dubin, C.Y. Chiu, R. Kaner, Y. Huang, X. Duan, Angew. Chem. Int. Ed. 51 (2012) 3822–3825.
[33] M. Duan, J. Li, G. Mele, C. Wang, X. Lu, G. Vasapollo, F. Zhang, J. Phys. Chem. C 114 (2010) 7857–7862.
[34] Q. Wang, Z. Yang, X. Zhang, X. Xiao, C.K. Chang, B. Xu, Angew. Chem. Int. Ed. 46 (2007) 4285–4289.
[35] V.P. Barros, A.L. Faria, T.C.O. MacLeod, L.A.B. Moraes, M.D. Assis, Int. Biodeter. Biodegr. 61 (2008) 337–344.
[36] Y. Huang, W. Ma, J. Li, M. Cheng, J. Zhao, J. Phys. Chem. B 107 (2003) 9409–9414.
[37] F. Dong, L. Wu, Y. Sun, M. Fu, Z. Wu, S.C. Lee, J. Mater. Chem. 21 (2011) 15171.
[38] X. Zhang, X. Xie, H. Wang, J. Zhang, B. Pan, Y. Xie, J. Am. Chem. Soc. 135 (2013) 18–21.
[39] F. Dong, Y. Sun, L. Wu, M. Fu, Z. Wu, Catal. Sci. Technol. 2 (2012) 1332.
[40] F. Dong, Z. Wang, Y. Sun, W.K. Ho, H. Zhang, J. Colloid Interface Sci. 401 (2013) 70–79.
[41] W. Ho, Z. Zhang, W. Lin, S. Huang, X. Zhang, X. Wang, Y. Huang, ACS Appl. Mater. Interfaces 7 (2015) 5497–5505.
[42] A. Thomas, A. Fischer, F. Goettmann, M. Antonietti, J.-O. Müller, R. Schlögl, J.M. Carlsson, J. Mater. Chem. 18 (2008) 4893.
[43] J. Li, B. Shen, Z. Hong, B. Lin, B. Gao, Y. Chen, Chem. Commun. 48 (2012) 12017–12019.
[44] J. Zhang, M. Zhang, G. Zhang, X. Wang, ACS Catal. 2 (2012) 940–948.
[45] G. Faubert, G. Lalande, R. Côté, D. Guay, J.P. Dodelet, L.T. Weng, P. Bertrand, G. Dénès, Electrochim. Acta 41 (1996) 1689–1701.
[46] K. Nilson, P. Palmgren, J. Åhlund, J. Schiessling, E. Göthelid, N. Mårtensson, C. Puglia, M. Göthelid, Surf. Sci. 602 (2008) 452–459.
[47] S. Yang, Y. Gong, J. Zhang, L. Zhan, L. Ma, Z. Fang, R. Vajtai, X. Wang, P.M. Ajayan, Adv. Mater. 25 (2013) 2452–2456.
[48] H. Bader, V. Sturzenegger, J. Hoigne, Water Res. 22 (1988) 1109–1115.
[49] S.-Y. Pang, J. Jiang, J. Ma, Environ. Sci. Technol. 45 (2011) 307–312.
[50] C. Tai, J.-F. Peng, J.-F. Liu, G.-B. Jiang, H. Zou, Anal. Chim. Acta 527 (2004) 73–80.
[51] M.R. Bukowski, K.D. Koehntop, A. Stubna, E.L. Bominaar, J.A. Halfen, E. Munck, W. Nam, Q. L Jr., Science 310 (2005) 1000–1002.
[52] P.D. Oldenburg, Y. Feng, I. Pryjomska-Ray, D. Ness, Q. L Jr., J. Am. Chem. Soc. 132 (2010) 17713–17723.
[53] J.T. Groves, R.C. Haushalter, M. Nakamura, T.E. Nemo, B.J. Evans, J. Am. Chem. Soc. 103 (1981) 2884–2886.
[54] M. Nango, T. Iwasaki, Y. Takeuchi, Y. Kurono, J. Tokuda, R. Oura, Langmuir 14 (1998) 3272–3278.
[55] W. Nam, H.J. Han, S.-Y. Oh, Y.J. Lee, M.-H. Choi, S.-Y. Han, C. Kim, S.K. Woo, W. Shin, J. Am. Chem. Soc. 122 (2000) 8677–8684.
[56] C. Chen, W. Ma, J. Zhao, Chem. Soc. Rev. 39 (2010) 4206–4219.
[57] S. Ge, L. Zhang, Environ. Sci. Technol. 45 (2011) 3027–3033.
[58] M. Kong, Y. Li, X. Chen, T. Tian, P. Fang, F. Zheng, X. Zhao, J. Am. Chem. Soc. 133 (2011) 16414–16417.
[59] Q. Xiang, J. Yu, M. Jaroniec, J. Phys. Chem. C 115 (2011) 7355–7363.
[60] J. Zhang, G. Zhang, X. Chen, S. Lin, L. Mohlmann, G. Dolega, G. Lipner, M. Antonietti, S. Blechert, X. Wang, Angew. Chem. Int. Ed. 51 (2012) 3183–3187.
[61] T. Sano, S. Tsutsui, K. Koike, T. Hirakawa, Y. Teramoto, N. Negishi, K. Takeuchi, J. Mater. Chem. A 1 (2013) 6489.